Lab on a Chip

Accepted Manuscript

ROYAL SOCIETY OF CHEMISTRY

www.rsc.org/loc

Lab on a Chip

ARTICLE

Microfluidic device to control interstitial flow-mediated homotypic and heterotypic cellular communication

Received 4th May 2015,
Accepted 00th January 20xx

DOI: 10.1039/x0xx00000x

www.rsc.org/

Luis F. Alonzo,[c] Monica L. Moya,[c] Venktesh S. Shirure[a] and Steven C. George†[a,b]

Tissue engineering can potentially recreate *in vivo* cellular microenvironments *in vitro* for an array of applications such as biological inquiry and drug discovery. However, the majority of current *in vitro* systems still neglect many biological, chemical, and mechanical cues that are known to impact cellular fucntions such as proliferation, migration, and differentiation. To address this gap, we have developed a novel microfluidic device that precisely controls the spatial and temporal interactions between adjacent three-dimensional cellular environments. The device consists of four interconnected microtissue compartments (~0.1 mm^3) arranged in a square. The top and bottom pairs of compartments can be sequentially loaded with discreate cellularized hydrogels creating the opportunity to investigate homotypic (left to right or x-direction) and heterotypic (top to bottom or y-direction) cell-cell communication. A controlled hydrostatic pressrure difference across the tissue compartments in both x and y direction induces inerestitial flow and modulates communication via soluble factors. To validate the biological significance of this novel platform, we examined the role of stromal cells in the process of vasculogenesis. Our device confirms previous observations that soluble mediators derived from normal human lung fibroblasts (NHLFs) are necessary to form a vascular network derived from endothelial colony forming cell-derived endothelial cells (ECFC-ECs). We conclude that this platfrom could be used to study important physiological and pathological processes that rely on homotypic and heterotypic cell-cell communication.

Introduction

Our vast understanding of cellular function has been largely gleaned from monotypic cell culture in 2D. This approach, however, neglects many biological, chemical, mechanical, and geometrical cues within the *in vivo* microenvironment that are known to impact important cellular functions such as proliferation, migration, and differentiation.

Embedding cells within an extracellular matrix (ECM) – naturally-derived or synthetic – is a common technique to mimic the 3D microenvironment. These 3D methods can create an ECM with tunable parameters to specifically control matrix density, stiffness, density of binding domains, and protein composition. Culturing cells in 3D environments not only serves to better recapitulate spatially the *in vivo* environment but also provides important biomechanical cues. As a result, cells employ alternate signaling pathways when cultured in 3D [1–4], which in turn affects cellular phenotype, growth, and migration [5–7]. This approach has made important contributions to our understanding of tumor development, capillary morphogenesis, among other cellular activities.

In addition to being 3D, the microenvironment of most tissues is characterized by a heterogeneous cell population. Cells do not live in isolation, but rather interact with neighboring cells of the same (homotypic) or different (heterotypic) type. The interaction can be either through direct cell-cell contact or through the secretion of soluble mediators (paracrine signaling). For example, capillary morphogenesis and liver function strongly depend on heterotypic communication between endothelial cells, hepatocytes, and neighboring stromal cells [8–15]. Tumor cell progression also depends strongly on heterotypic cell-cell interaction with surrounding "normal" cells such as the fibroblast and infiltrating immune cells [16–20].

Biomechanical forces in the cellular microenvironment, such as interstitial flow, can also modulate cellular behavior. Interstitial flow not only directly influences cell function by engaging mechanosensors on the cell surface through both normal and shear stress, it can also impact extracellular gradients of soluble mediators and enhances transport of nutrients and waste, which can indirectly impact cellular processes [21–23]. Physiological interstitial flow has been shown to be in the range of 0.1-2 um/s [24]; however, supra- and sub-physiological flow *in vitro* (0.01-100 um/s)can drive vascular network formation in disease states such as cancer [25,26].

Current *in vitro* systems do not simultaneously employ and control heterotypic and homotypic cellular communication, and interstitial fluid forces. In this research, we have the spatial and temporal interactions between adjacent

[a] *Department of Biomedical Engineering, Washington University in St. Louis, MO 63130*
[b] *Department of Energy, Environment, and Chemical Engineering, Washington University in St. Louis, MO 63130*
[c] *Department of Biomedical Engineering, University of California, Irvine, CA 92697.*
† Washington University in St. Louis, 1 Brookings Drive, Campus Box 1097, St. Louis, MO 63130, USA. E-mail: scg@wustl.edu; Telephone: +1 314 935 4588

heterotypic and homotypic cellular environments. The communication ports, a special feature of the device, have been specifically designed to control the loading of two discrete, but interconnected, 3D cell-containing hydrogels. In addition, hydrostatic pressure forces across the 3D tissues create interstitial flow that controls endogenous and/or exogenous soluble factor concentration and spatial gradients. We demonstrate the utility of his platform to control heterotypic cellular communication in vasculogenesis, and anticipate that this platform could be used to study other important physiological and pathological processes (e.g. tumor progression).

Materials and Methods

Cell culture

Human endothelial colony forming cell-derived – endothelial cells (ECFC-ECs) were derived from cord blood as previously described by our lab [27] and expanded on 1% gelatin-coated flasks in endothelial growth medium-2 (EGM-2; Lonza, Wakersfield, MD). ECFC-ECs were use at passages 4-6 during the experiments. Commercially available normal lung human fibroblasts (NHLFs; Lonza) were grown in fibroblast growth media (FGM-2; Lonza) and used at passages 5-7. For NHLF-conditioned media experiments, FGM-2 media was removed the day before and replaced with EGM-2 media overnight. On experiment day, the conditioned media was collected and filtered of any cellular debris. All cells were cultured in a humidified incubator at 37^{o}C, 5% CO_2, and 20% O_2 prior to introduction in the 4-chambered microfluidic device.

Lentiviral transduction of NHLFs to constitutively express fluorescence

To study the invasiveness of NHLFs, we transduced the cells with a titer of a lentiviral vector produced in HEK293T cells. To prepare the vector, HEK293T cells were cultivated in a 6-well plate at a concentration of 5.0×10^5 cells/well in DMEM containing 10% fetal bovine serum (FBS) and depleted of sodium pyruvate (NaP). The cells were allowed to incubate for 24 hours at 37^{o}C with humidified air containing 5% CO_2. Following the incubation period, a solution containing 250 µL of Opti-MEM (Invitrogen) and 6 µg of plasmid DNA (1.5 µg pLVX-mCherry-C1, Clontech, Mountain View, CA, 0.75 µg pMDLg/pPRE, Addgene, Cambridge, MA , 0.3 µg pRSV-Rev, Addgene, Cambridge, MA , and 0.45 µg pMD2.G; Addgene, Cambridge, MA), and a solution of 7.5 µL of Lipofectamine 2000 (Invitrogen) and 250 µL of Opti-MEM were prepared. Both solutions were mixed together and incubated at room temperature for 25 minutes. 500 µl was added drop-wise to each well containing HEK293T cells. After 24 hours, the content of each well was replaced with fresh DMEM. After 48 hours, the supernatant containing the virus was collected, purified via centrifugation, and stored at -80^{o}C for further use.

A T-75 flask containing roughly 50% confluent NHLFs was incubated overnight with a mixture of 2 mL of the viral titer, 6 µL of 10 mg/mL polybrene (Milipore, Billerica, MA), and 8 mL of DMEM. The resulting transduction efficiency was measured to be greater than 90%.

Microfluidic device design and fabrication

The microfluidic device design consists of two discrete rows (a top row and a bottom row) of tissue channels (Figure 1B). Each row contains two daisy-chained chambers (1 mm × 1 mm x 0.1 mm = 0.1 mm^3) connected in series through one pore measuring 30 µm wide and 100 µm high. The two rows of tissue channels were loaded separately with cell-containing hydrogels resulting in a pair of daisy-chained chambers containing an identical cellular composition. Thus, if only one cell type was present in a row, communication between the chambers would be homotypic. In turn, the two tissue chambers in the top row were connected to the corresponding chamber in the bottom row through 2 pores measuring 30 µm wide and 100 µm high. The micropores were specifically designed to mimic a capillary burst valve [25,26,28], which aids in the patterning of each row with a hydrogel sequentially within the device; that is, the top row can be loaded first, followed by the loading of the bottom row (Figure 1C). In this fashion, the cellular composition of the bottom row can be different than the top row resulting in heterotypic cell-cell communication. In addition, either side of the 4-chambered region that houses the 3D cellular microenvironments was connected to fluid-filled microchannels via two pores using the same geometry of the previously described capillary burst valve (Figure 1B). The pressure, flow, and composition of each microfluidic channel were controlled independently to provide a dynamic supply of media to the microtissue chambers by diffusion and convection.

Standard soft lithography and replica molding processes were utilized to fabricate the 4-chambered microfluidic device. In brief, a master mold was created via ultraviolet patterning of a 100 µm thick photoresist, SU-8 (MicroChem, Newton, MA), on a silicon wafer. A polydimethylsiloxane (PDMS; Dow Corning, Elizabethtown, KY) mixture composed of 10:1 (w/w) base to curing agent was poured over the master mold and thermally cured at 65^{o}C overnight. Once fully cured, the PDMS was cut and peeled off the mold; leaving a negative imprint of the 4-chambered design. Inlet and outlet holes were punched in the PDMS piece to allow for extracellular matrix (ECM) and cell culture media injection. All debri was removed from the PDMS piece, followed by oxygen plasma treatment for 3.5 minutes at 250 mTorr. A 500-750 µm thick PDMS sheet and a 130-170 µm thick glass coverslip (Thermo Fisher Scientific, Waltham, MA) were simultaneously plasma treated and covalently bonded to the PDMS piece to seal the channels of the PDMS device and provide mechanical support, respectively. The completed device was then baked at 120^{o}C for a few minutes to invert the hydrophilic properties acquired during the plasma treatment process. Finally, the device was autoclaved at 120^{o}C to sterilize and prepare the device for the experiment.

Cell loading in microfluidic device

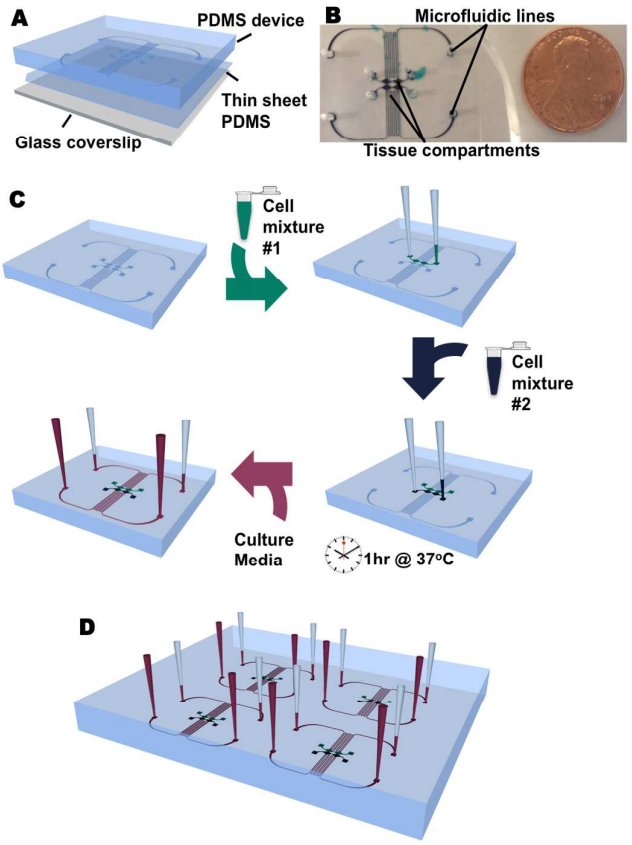

Figure 1. Four-chambered microfluidic device to study interstitial flow-driven communication between discrete microenvironments. (A) An illustration of the components of the microfluidic device. PDMS enclosed chambers are obtained by irreversibly plasma bonding the PDMS device to a thin sheet of PDMS and a glass coverslip. (B) A macroscopic view of the device shows two distinct tissue compartments – where the cell containing hydrogels are housed - connected in parallel, as well as the adjacent microfluidic lines which allow for the introduction of cell culture media. (C) Schematic of the device's loading process. Two distinct cell containing hydrogels may be manually injected sequentially into their respective tissue compartments using a micropipetter. After the hydrogels have polymerized, cell culture media can be similarly injected into the adjacent microfluidic lines. The pipette tips used to inject the media are then used to create a hydrostatic pressure gradient across the tissue compartments by adjusting the volume of media in each of the tips every ~24 hours for the remainder of the experiment. (D) Each custom made platform is designed to hold four separate devices.

For tissue preparation, cells were trypsinized and resuspended in 10 mg/ml bovine fibrinogen (Sigma-Aldrich, St. Louis, MO) dissolved in 1x Dulbecco's Phosphate Buffered Saline (DPBS; Gibco). Four different cellular conditions were mixed with the fibrinogen solution at a final concentration of 2.5×10^6 ECFC-ECs/mL and 5.0×10^6 NHLFs/mL. Thrombin (Sigma-Aldrich) was added to the cell-fibrinogen mixture to a final concentration of 3 U/mL to begin the gel polymerization process, and the solution was pipetted quickly into the tissue compartments of the PDMS device. Each one of the two tissue compartments was carefully loaded in a sequential order creating two identical tissue compartments on the top row of the device, and two identical tissue compartments on the bottom row. The device was then incubated at 37 °C for 1 hr to finalize the fibrin polymerization. EGM-2 media or NHLF conditioned media was then pipetted into the microfluidic lines adjacent to each of the tissue compartments. The volume of each pipette tip was adjusted to create the desired pressure gradient across the tissue, and the microfluidic platform was placed in a 20% O_2 incubator for 7 days. Media volumes were adjusted every 24 hr to maintain a nearly constant pressure head (gradient) for the duration of the experiment.

Finite element simulation

The experimental fluid flow and pressures were simulated using COMSOL Multiphysics® 3.5a (Burlington, MA). A computer-aided design (CAD) model of the 4-chambered microfluidic device was constructed and solved using a 2D steady state solution of the incompressible Navier-Stokes equation. All surfaces, except the inlet and outlet, were assumed to have a no-slip boundary condition. Other initial conditions specified in the simulation were: dynamic viscosity of water, 0.748 mPa·s; density of water, 1 kg/m^3; porosity of fibrin gel, 0.99; and permeability of fibrin gel, 1.5×10^{-13} m^2, consistent with our previous work [25,26,29]. The resulting pressure and velocity field simulations were used to design the magnitude and pattern of convection and diffusion in the microfluidic device.

Verification of mass transport

Fluorescent recovery after photobleaching (FRAP) was used to measure experimentally the flow across the fibrin gel using a modified protocol [30,31]. Both tissue compartments of the 4-chambered microfluidic device were loaded with a 10 mg/ml fibrin gel in the absence of cells. FITC-dextran (70 kDa, Sigma-Aldrich) was added to the adjacent fluidic lines via pipette tips. Volumes of the FITC-dextran containing solution were then readjusted to achieve two distinct interstitial flow profiles modeled in COMSOL. FRAP was then performed on the device at the junctions connecting each tissue chamber using a confocal microscope (Zeiss LSM 700, Carl Zeiss AG, Feldbach, Switzerland). A circular region of 30 µm was bleached, and images were taken every half a second for a total of 30 seconds. The location of the centroid of the bleached spot depends only on convection (i.e., is independent of random Brownian motion or diffusion); thus, the distance traveled by the centroid in a given time was to calculate the convective velocity of fluid flow in the device.

Assessment of vessel network formation

After 7 days of culture, vessel networks formed in the microtissues were immunofluorescently labeled using a modified staining protocol [26,27]. The microtissues were initially fixed in 10% formalin that was introduced through the adjacent microfluidic channels for 18 hrs. The staining process consisted of exposing the microtissues to mouse anti-human CD31 (a surface marker of endothelial cells) antibody (Dako, Carpinteria, CA) for 1-2 days, followed by Alexa-Flour 488-conjugated goat anti-mouse IgG (Invitrogen, Grand Island, NY) for an additional 1-2 days. Images of the stained microvessels were taken using an inverted fluorescence microscope (Olympus IX83, Central Valley, PA). Vessels staining positive for CD31 were analyzed using AngioTool [32], a software for

quantitative assessment of vessel networks. A previously defined index of network connectedness was calculated using results from the AngioTool analysis [26]. Using this index, values approaching 0 indicate a well-connected network.

Experimental design

The experimental design is summarized in Figure 2. To create a longitudinal interstitial flow pattern (x-direction), the design of the fluid-filled microchannels employs a serpentine configuration, which offers an increased resistance to media flow between the 2 pore connections to manipulate the pressure across the tissue chamber, and thus the mass transport within the 4-chambered region. In this configuration, the pattern of the media flow is across the tissue chambers in series, by having high pressure on the left side of the tissue chamber and low pressure on the right side. The transverse interstitial flow configuration (y-direction) is set up to allow media flow across the tissue chambers in parallel to span from the top tissue chamber (Figure 2 – green channel) up to the bottom tissue chamber (Figure 2 – blue channel), by having a high pressure on the top side and a low pressure on the bottom side. To examine the impact of heterotypic cell-cell communication on vasculogenesis, we tested four different conditions (Figure 2).

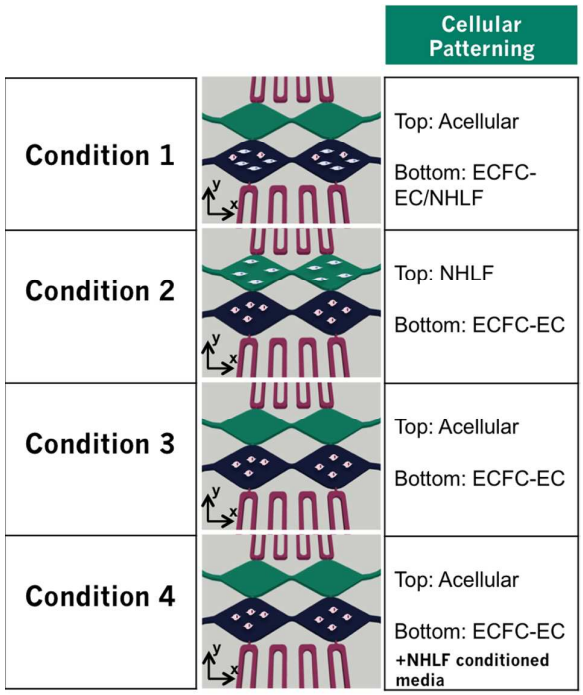

Figure 2. Cellular seeding pattern and interstitial flow experimental conditions. The microfluidic device is amenable to diverse experimental culturing conditions due to the inherent ability to control the cellular composition within each tissue compartment (green and blue channels) and the communication between the compartments through the regulation of interstitial flow direction. For the purpose of validating the device, this study examined the role of stromal cells in vessel network formation; therefore, ECFC-ECs were 1) co-cultured within the same tissue chamber with NHLFs, 2) co-cultured in the adjacent tissue chamber separately connected to NHLFs, 3) cultured in the absence of NHLFs, or 4) cultured in the presence of NHLF pre-conditioned media only. Two types of cellular communications are possible: heterotypic and homotypic cell-cell communication. Heterotypic cellular communication between the two discrete compartments in parallel (green and blue channels) can be achieved by adjusting the volumes of the pipette tips to obtain an interstitial flow pattern in the transverse direction (y-axis). Similarly, a homotypic cellular communication between the two diamond-shaped compartments in series (green only or blue only channels) can be achieved by adjusting the volumes of the pipette tips to obtain an interstitial flow pattern in the longitudinal direction (x-axis).

Statistical analysis

Statistical analysis was performed using one-way analysis of variance (ANOVA) with StatPlus (AnalystSoft Software). Post-hoc comparisons between groups were made with the Tukey test for multiple comparisons. All data are presented as the mean ± standard deviation. Results were considered statistically significant for $p < 0.05$.

Results

Microfluidic device

Two distinct fibrin gels (TRITC and FITC labeled) can be loaded in the top and bottom row sequentially (Figure 3A). The result is a continuous 3D environment between the two tissue compartments on the top and bottom rows. To simulate a transverse (top to bottom or y-axis) interstitial convective flow pattern, a ΔP of 20 mmH_2O was applied from position α to position β, as well as α' to β' (Figure 3B). Here the pressure within the top and bottom microfluidic lines is constant at a high and low pressure, respectively. The pressure within the microtissue chambers decreases in the transverse direction (Figure 3B) resulting in flow that is predominantly in the transverse direction (Figure 3C). The simulated fluid velocity in the pore region reached a maximum value of ~190 µm/s and an average value of 100 µm/s over a 200 µm distance from the center of the pore (Figure 3D). The minimal convective flow and diffusion limited by the narrow pores linking the chambers in each row significantly limits the mass transfer of soluble factors in the longitudinal direction. As a result, there is no appreciable communication between the chambers in the longitudinal direction (Figure S1C).

Alternatively, to simulate a longitudinal interstitial flow pattern, a ΔP of 20 mmH_2O was applied from α to α', as well as β to β' (Figure 3E). A decrease in pressure is observed within the microfluidic lines moving left to right resulting in a decrease in the pressure within the microtissue chambers from the left column to right column. The simulated streamlines (Figure 3F) demonstrate that flow is predominantly in the longitudinal direction (left to right or along the x-axis) as flow enters from the microfluidic line into the left chamber, flows left to right into the right chamber and then exits into the microfluidic line. There is no appreciable communication between the parallel (top to bottom or y-axis) chambers (Figure S1F). It is important to note that the design of the two discrete tissue channels includes a region where the area is reduced to 30 µm. This geometrical configuration accelerates the interstitial fluid between the two chambers in series in order to conserve mass for an incompressible fluid. The simulated fluid velocity in the pore region reached a maximum value of ~40 µm/s and an average value of 25 µm/s over a 200 µm distance from the center of the pore (Figure 3G).

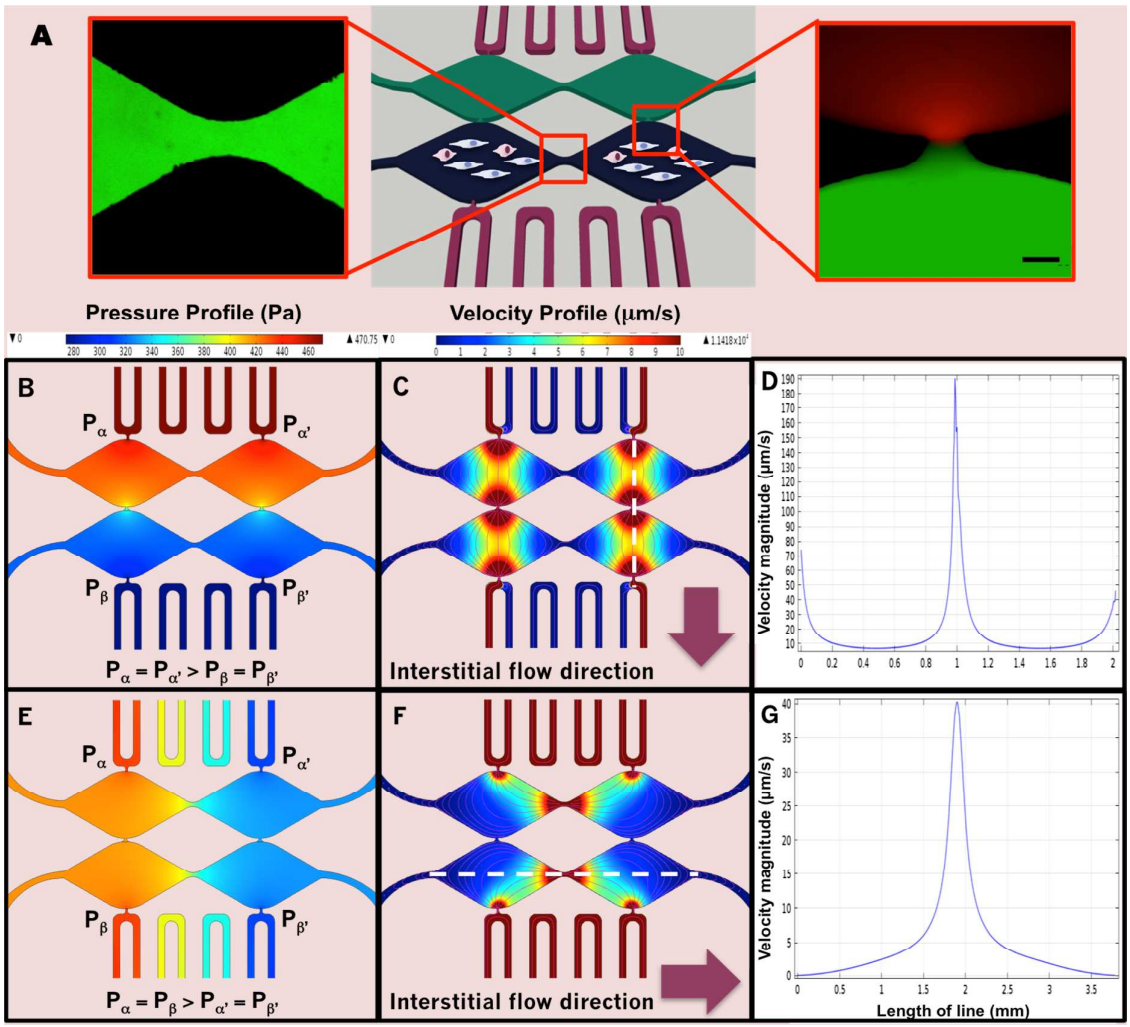

Figure 3. Finite element simulations demonstrate control of pressure distribution and associated interstitial flow distribution within the microfluidic device. (A) A continuous 3D environment can be achieved through the sequential loading of the tissue compartments (TRITC and FITC labeled) which allows for the uninterrupted communication between adjacent compartments. (B-D) Heterotypic communication between the two compartments in parallel can be achieved by setting a pressure difference (ΔP) between the top microfluidic channel and the bottom microfluidic channel ($P_\alpha = P_{\alpha'} > P_\beta = P_{\beta'}$), which results in a transverse (y-axis) interstitial convective flow pattern. Theoretical fluid flow velocities along the length of the two compartments aligned with the direction of flow is shown (white dotted line). (E-G) Homotypic communication between the diamond-shaped compartments in series can be achieved by setting a ΔP between the left sides of the top/bottom and the right sides of the top/bottom of the microfluidic lines ($P_\alpha = P_\beta > P_{\alpha'} = P_{\beta'}$), which results in a longitudinal (x-axis) interstitial convective flow pattern. Theoretical fluid flow velocities along the length of the two compartments aligned with the direction of flow is shown (white dotted line). Scale bar: 30 um.

Fluorescence recovery after photobleaching (FRAP) has been widely used to study the mobility of macromolecules in various medias and tissues [30,33]. Using this technique, we surveyed two regions of the device to validate our simulation of flow: 1) the tapering pore between the tissue chambers in series (in the same row), and 2) the connecting pore between the top and bottom tissue chambers in parallel (in the same column) (Figure 4). These two regions represent the most extreme interstitial flow velocities. After generating a pressure gradient of 20 mmH_20 in the longitudinal direction (P_α-$P_{\alpha'}$ = P_β-$P_{\beta'}$ = 20 mmH_20) of flow, the fluid flow velocity within the fibrin gel was 69 μm/s in the longitudinal direction within the region connecting the top row of microtissue chambers (Figure 4A) while it was negligible in the region between the chambers in parallel (< 0.1 μm/s). Notably, the minor recovery of the bleached spot in these experiments also occurs due to diffusive transport of the molecules. Therefore, the centroid of the bleached spot, which is not affected by diffusion, was used to calculate the convective velocity. Alternatively, when a transverse pressure gradient was applied (P_α-P_β = $P_{\alpha'}$-$P_{\beta'}$ = 20 mmH_20), the fluid flow velocity within the fibrin gel was 8 μm/s at the pore between the chambers in parallel (Figure 4B), while it was negligible (< 0.1 μm/s) in the pore region between the two chambers in series. Small differences between experimental and theoretical fluid flow velocity values may be attributed to parameter values used in the simulation.

Vasculogenesis and inter-chamber communication

To show the versatility of our platform we manipulated interstitial flow to investigate the effect of heterotypic cell-cell communication on the process of vasculogenesis. It is known that interstitial flow can stimulate vasculogenesis and influence vessel formation through the redistribution of cell-secreted morphogens [22]. To this end, we examined four

different cellular patterning conditions to investigate the role of stromal cell-derived soluble mediators in the morphogenesis of microvessel networks.

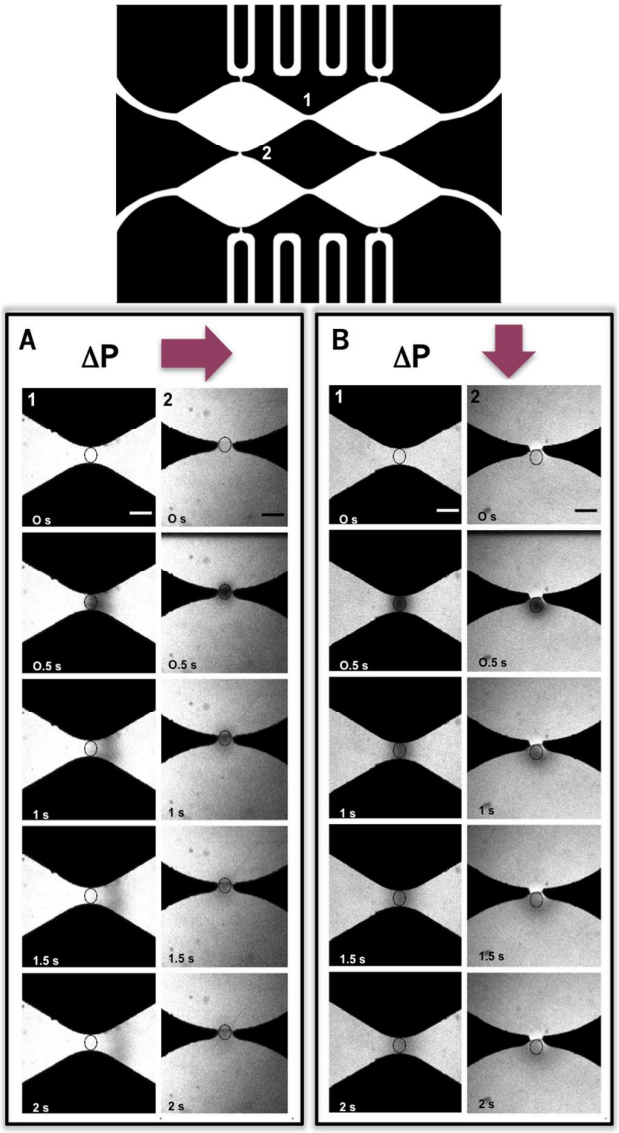

Figure 4. Fluorescence recovery after photobleaching (FRAP) validates simulated interstitial flow velocity results. FRAP was used to determine the local flow velocities at two regions within the tissue compartments (#1, #2) where the COMSOL simulations yielded the most extreme interstitial flow velocities. The black circles indicate the originally bleached area, and arrows indicate the direction of the bulk interstitial convective flow. (A) In the case of longitudinal interstitial flow (x-axis), the flow velocity was measured to be 69 μm/s at the junctions which connect the two diamond-shaped compartments in series (#1), while the velocity at the junctions which connect the two tissue compartments in parallel (#2) was negligible. (B) In contrast, when a transverse interstitial flow (y-axis) was applied, the flow velocity at spot #2 was measured to be 8 μm/s, while it remained negligible at spot #1. Scale bars: 50 um.

Figure 5 presents both the qualitative and quantitative features of the *in vitro* vessel networks formed within the lower right compartment of the microfluidic device under a series of longitudinal and transverse interstitial flow configurations. In devices where the bottom tissue compartment contained both ECFC-ECs and NHLFs (condition 1; Figure 5A,B), a robust and interconnected network of vessels (Figure 5J-K) formed in a similar fashion for both interstitial flow conditions tested (i.e., connectedness value of 0.64 ± 0.34 in longitudinal flow and 0.49 ± 0.25 in transverse flow). In devices where ECFC-ECs were seeded alone, non-continuous vascular structures were observed when exposed to the longitudinal flow condition (connectedness value of 14.08 ± 9.43 for condition 2, 15.23 ± 8.35 in condition 3, and 8.57 ± 5.56 in condition 4; Figure 5D,F,H), as well as in the transverse flow condition in the absence of any exogenous factors (connectedness value of 16.07 ± 10.34, Figure 5C). However, as the interstitial flow condition was adjusted to allow for ECFC-EC exposure to soluble factors originating from the NHLFs or conditioned media (i.e., transverse flow), an interconnected network was restored (i.e., connectedness value of 1.41 ± 0.47 for condition 3 and 1.20 ± 0.69 for condition 4; Figure 5E,G). In other words, significant vessel networks (by three indices, Figure 5I-K) in the lower right chamber formed only in the conditions in which soluble mediators from the NHLFs were transported to the ECFC-ECs either by diffusion in close approximation within the same chamber (Figure 5A, and B) or convection of interstitial flow from an adjacent compartment (Figure 5E, and G). mCherry fluorescence signal, originating from the NHLFs, was undetected in the ECFC-EC containing tissue compartments; verifying that no migratory effects played a role in these observations within the time course of the experiments (Figure S2).

Discussion

One of the goals of tissue engineering is the creation of *in vitro* tissue constructs that can recapitulate important features of the *in vivo* microenvironment. In this study, we have developed a novel microfluidic device, which simultaneously employs and controls heterotypic and homotypic cellular communication, and interstitial fluid forces. For this particular application, we have controlled the spatial arrangement of 3D fibrin gels containing mixed populations of endothelial and stromal cells. In addition, through simple hydrostatic pressure manipulations, we control the interstitial flow direction and thus paracrine signaling between adjacent and distinct cellular microenvironments. Using vessel network formation from heterotypic interactions between endothelial and stomal cells, we demonstrate the biological relevance of the platform.

The novelty of this device lies in the ability to precisely control the initial spatial and temporal interactions between adjacent heterotypic and homotypic cellular environments. Traditionally, Boyden chambers have been used to examine heterocellular interactions between cells, but most of these studies involve 2D culture conditions [34]. However, recent studies have modified the Boyden chamber assay to incorporate 3D microenvironments [35]. These systems are generally easy to use, but still do not allow fine spatial and temporal control of cells and matrix in 3D. Our platform can simply and reliably accommodate two adjacent 3D cell-containing hydrogels by taking advantage of capillary burst valves [28]. These two

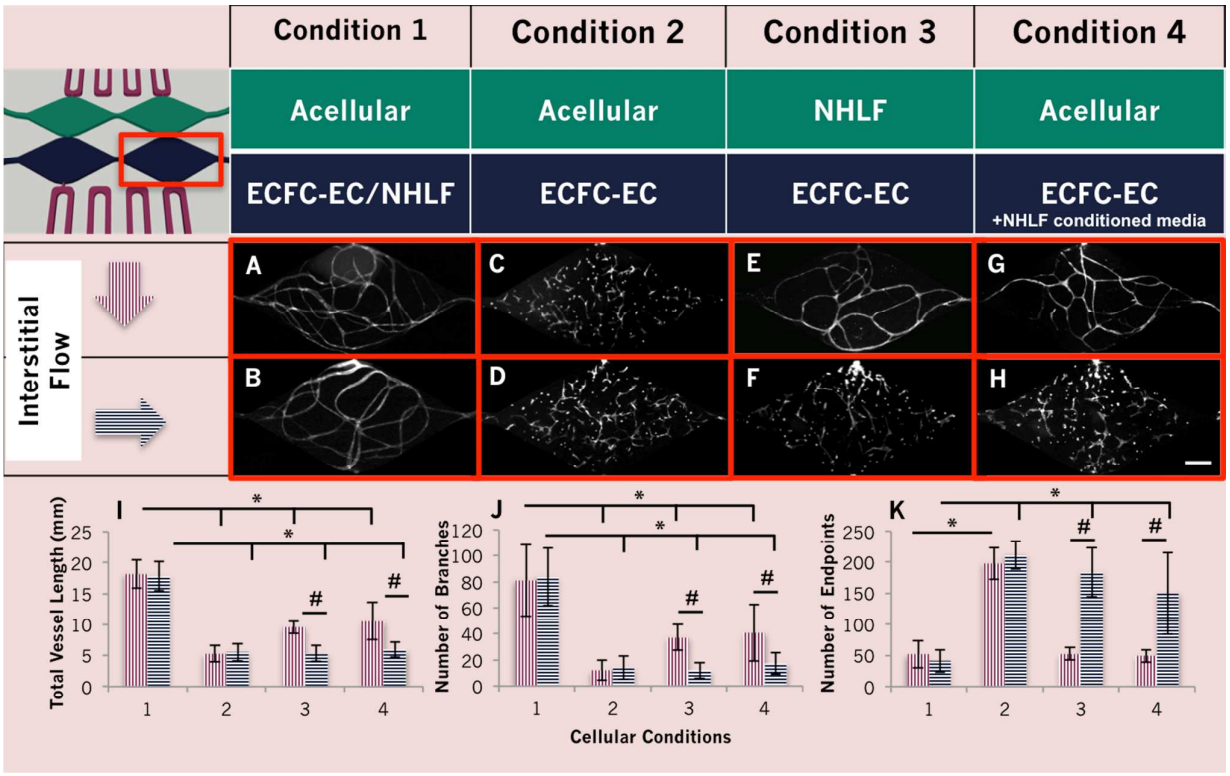

Figure 5. Formation of 3D *in vitro* interconnected vessel networks depends on interstitial flow-driven communication between ECFC-ECs and NHLFs. Qualitative confirmation of vessel network formation after 1 week of culture was conducted via fluorescently labeling ECFC-ECs with an anti-human CD31 antibody. (A-B) Significant vessel networks developed when ECFC-ECs and NHLFs were co-cultured within the same tissue compartment (condition 1) regardless of the direction of the interstitial convective flow. (C-D) However, under the same interstitial flow conditions and in the absence of NHLFs (condition 2), ECFC-ECs failed to form significant vessel networks. (F,H) Similarly, when NHLFs were cultured in a separate compartment or when NHLF conditioned media was introduced, but the interstitial flow direction was arranged to restrict ECFC-ECs' exposure to NHLF soluble mediators, no significant vessel network formation occurred. (E-G) Significant vessel network formation can be rescued when the interstitial flow direction is setup to allow for ECFC-ECs to be exposed to NHLF soluble mediators from adjacent NHLFs or pre-conditioned media. (I-K) Qualitative observations were confirmed through the quantitative analysis of standard indices measured from the resulting vessel networks. Total vessel length and number of branches peaked for cellular condition 1, significantly different from conditions 2, 3 and 4 under in both interstitial flow directions (*, $p<0.05$). In addition, parameters show significant difference between the two interstitial flow directions for conditions 3 and 4 (i.e. ECFC-EC exposure to NHLF soluble mediators; #, $p<0.05$). Scale bar: 100 um.

compartments are loaded independently, which provides the ability to culture one gel in isolation over a period of time prior to introducing the secondary tissue compartment of interest, as needed.

Even though physiological interstitial velocities are relatively low *in vivo* [24], the role of convection in the overall distribution of solutes can be significant. For example, cell response has been reported to be influenced by morphogen gradients across a cell as low as 1% [36]. Traditional *in vitro* cell culture platforms do not attempt to replicate and control this feature. Through control of the hydrostatic pressure difference across the chambers (ΔP) and the design of the microfluidic channels, our device can dictate both the temporal and spatial pattern of interstitial flow, and thus the morphogen concentration, in the cellular microenvironment. Nearly constant fluid flow conditions were maintained in the device by replacing the media volumes in the inlet/outlet ports every 24 hours. ~100 µl of media was added to the inlet to compensate for a 10% reduction of volume and an equal amount of media was removed from the outlet corresponding to the increase of volume due to the fluid flow within the device over this time period. We studied two different interstitial flow configurations, the first allows communication between the chambers in series (longitudinal; homotypic cellular interactions) and the second allows for communication between the chambers in parallel (transverse; heterotypic cellular interactions).

Previous studies have demonstrated that the presence of stromal cells is critical for the formation of vessel networks *in vivo* and *in vitro* [8–11,27,37]. Our results matched well with these previous reports. In our device, significant vessel networks formed only in the conditions in which ECFC-ECs were exposed to soluble mediators released by NHLFs. This occurred in conditions were the two cell types were in close proximity as well as when they relied on interstitial flow-mediated communication while they were in physically separate microenvironments. These results validate the biological relevance of the device design.

While our studies have demonstrated the utility of our platform, we believe there are potentially broad diagnostic and therapeutic applications. For instance, the platform may be used to investigate the role of microenvironmental-derived paracrine factors in stem cell pluripotency, differentiation, and growth [38]. Similarly, one could investigate the role of heterotypic or homotypic cell communication on tumor growth and vascularization within the complex tumor microenvironment.

Conclusions

Our results demonstrate the utility of a novel microfluidic device that may be used to investigate homotypic and heterotypic cell-cell communication patterns in biologically relevant 3D microenvironments. In particular, we have shown the unique ability to investigate the role of paracrine signaling, which is modulated through the control of interstitial flow. A model of vasculogenesis was used to validate the device, but the system has the potential to be used as a broad tool for scientific discovery. The device provides flexibility and reproducibility in a controlled environment, and can allow for high-throughput screening, which may be useful for drug discovery.

Acknowledgements

This work was supported by grants from the National Institutes of Health (UH3 TR00048, R01 CA170879, F31 CA163049, F32 HL105055). The authors would like to thank Mo Kebaili at the UCI Integrated Nanosystems Research Facility (INRF) and Sandra Lam for their assistance fabricating the device's master molds. We would also like to thank Dr. Yu-Hsiang Hsu and Dr. Abraham Lee for their helpful advice and discussions during the development stages of this project. Finally, we would like to thank Linda McCarthy for her assistance with the cell transductions.

Notes and references

1 F. Pampaloni, E. G. Reynaud and E. H. K. Stelzer, *Nat. Rev. Mol. Cell Biol.*, 2007, **8**, 839–845.
2 Y.-C. Tung, A. Y. Hsiao, S. G. Allen, Y. Torisawa, M. Ho and S. Takayama, *Analyst*, 2011, **136**, 473–8.
3 B. Weigelt, A. T. Lo, C. C. Park, J. W. Gray and M. J. Bissell, *Breast Cancer Res. Treat.*, 2010, **122**, 35–43.
4 K. M. Yamada and E. Cukierman, *Cell*, 2007, **130**, 601–10.
5 G. Chen, Y. Lv, P. Guo, C. Lin, X. Zhang, L. Yang and Z. Xu, *Curr. Stem Cell Res. Ther.*, 2013, **8**, 313–23.
6 U. S. Schwarz and M. L. Gardel, *J. Cell Sci.*, 2012, **125**, 3051–60.
7 T. W. Kragstrup, M. Kjaer and A. L. Mackey, *Scand. J. Med. Sci. Sports*, 2011, **21**, 749–57.
8 D. Ribatti, B. Nico and E. Crivellato, *Int. J. Dev. Biol.*, 2011, **55**, 261–8.
9 N. Takakura, *J. Thromb. Haemost.*, 2011, **9 Suppl 1**, 144–50.
10 D. J. Crocker, T. M. Murad and J. C. Geer, *Exp. Mol. Pathol.*, 1970, **13**, 51–65.
11 P. C. Stapor, R. S. Sweat, D. C. Dashti, A. M. Betancourt and W. L. Murfee, *J. Vasc. Res.*, 2014, **51**, 163–74.
12 E. E. Hui and S. N. Bhatia, *Proc. Natl. Acad. Sci. U. S. A.*, 2007, **104**, 5722–5726.
13 E. E. Hui and S. N. Bhatia, *Langmuir*, 2007, **23**, 4103–4107.
14 S. N. Bhatia, M. L. Yarmush and M. Toner, *J. Biomed. Mater. Res.*, 1997, **34**, 189–199.
15 S. N. Bhatia, U. J. Balis, M. L. Yarmush and M. Toner, *Biotechnol. Prog.*, 1998, **14**, 378–387.
16 T. D. Tlsty and L. M. Coussens, *Annu. Rev. Pathol.*, 2006, **1**, 119–50.
17 J. A. Joyce and J. W. Pollard, *Nat. Rev. Cancer*, 2009, **9**, 239–52.
18 M. J. Bissell and D. Radisky, *Nat. Rev. Cancer*, 2001, **1**, 46–54.
19 G. P. Gupta and J. Massagué, *Cell*, 2006, **127**, 679–95.
20 M. Allinen, R. Beroukhim, L. Cai, C. Brennan, J. Lahti-Domenici, H. Huang, D. Porter, M. Hu, L. Chin, A. Richardson, S. Schnitt, W. R. Sellers and K. Polyak, *Cancer Cell*, 2004, **6**, 17–32.
21 C. L. E. Helm, A. Zisch and M. A. Swartz, *Biotechnol. Bioeng.*, 2007, **96**, 167–176.
22 C.-L. E. Helm, M. E. Fleury, A. H. Zisch, F. Boschetti and M. A. Swartz, *Proc. Natl. Acad. Sci. U. S. A.*, 2005, **102**, 15779–15784.
23 C. P. Ng, C. L. E. Helm and M. A. Swartz, *Microvasc. Res.*, 2004, **68**, 258–264.
24 M. A. Swartz and M. E. Fleury, *Annu. Rev. Biomed. Eng.*, 2007, **9**, 229–56.
25 Y.-H. Hsu, M. L. Moya, P. Abiri, C. C. W. Hughes, S. C. George and A. P. Lee, *Lab Chip*, 2013, **13**, 81–9.
26 M. L. Moya, Y.-H. Hsu, A. P. Lee, C. C. W. Hughes and S. C. George, *Tissue Eng. Part C. Methods*, 2013, **19**, 730–7.
27 X. Chen, A. S. Aledia, S. A. Popson, L. Him, C. C. W. Hughes and S. C. George, *Tissue Eng. Part A*, 2010, **16**, 585–94.
28 H. Cho, H. Y. Kim, J. Y. Kang and T. S. Kim, *J. Colloid Interface Sci.*, 2007, **306**, 379–385.
29 Y.-H. Hsu, M. L. Moya, C. C. W. Hughes, S. C. George and A. P. Lee, *Lab Chip*, 2013, **13**, 2990–8.
30 U. Haessler, J. C. M. Teo, D. Foretay, P. Renaud and M. A. Swartz, *Integr. Biol. (Camb).*, 2012, **4**, 401–9.
31 C. Bonvin, J. Overney, A. C. Shieh, J. B. Dixon and M. A. Swartz, *Biotechnol. Bioeng.*, 2010, **105**, 982–91.
32 E. Zudaire, L. Gambardella, C. Kurcz and S. Vermeren, *PLoS One*, 2011, **6**.
33 R. K. Jain, R. J. Stock, S. R. Chary and M. Rueter, *Microvasc. Res.*, 1990, **39**, 77–93.
34 S. BOYDEN, *J. Exp. Med.*, 1962, **115**, 453–466.
35 J. D. Shields, M. E. Fleury, C. Yong, A. A. Tomei, G. J. Randolph and M. A. Swartz, *Cancer Cell*, 2007, **11**, 526–38.
36 S. H. Zigmond, *J. Cell Biol.*, 1977, **75**, 606–616.
37 X. Chen, A. S. Aledia, C. M. Ghajar, C. K. Griffith, A. J. Putnam, C. C. W. Hughes and S. C. George, *Tissue Eng. Part A*, 2009, **15**, 1363–71.
38 A. Khademhosseini, L. Ferreira, J. Blumling, J. Yeh, J. M. Karp, J. Fukuda and R. Langer, *Biomaterials*, 2006, **27**, 5968–77.